

## UvA-DARE (Digital Academic Repository)

### Comprehensive study of the macropore and mesopore size distributions in polymer monoliths using complementary physical characterization techniques and liquid chromatography

Wouters, S.; Hauffman, T.; Mittelmeijer-Hazeleger, M.C.; Rothenberg, G.; Desmet, G.; Baron, G.V.; Eeltink, S.

#### DOI

[10.1002/jssc.201600896](https://doi.org/10.1002/jssc.201600896)

#### Publication date

2016

#### Document Version

Final published version

#### Published in

Journal of Separation Science

#### License

Article 25fa Dutch Copyright Act (<https://www.openaccess.nl/en/policies/open-access-in-dutch-copyright-law-taverne-amendment>)

[Link to publication](#)

#### Citation for published version (APA):

Wouters, S., Hauffman, T., Mittelmeijer-Hazeleger, M. C., Rothenberg, G., Desmet, G., Baron, G. V., & Eeltink, S. (2016). Comprehensive study of the macropore and mesopore size distributions in polymer monoliths using complementary physical characterization techniques and liquid chromatography. *Journal of Separation Science*, 39(23), 4492-4501. <https://doi.org/10.1002/jssc.201600896>

#### General rights

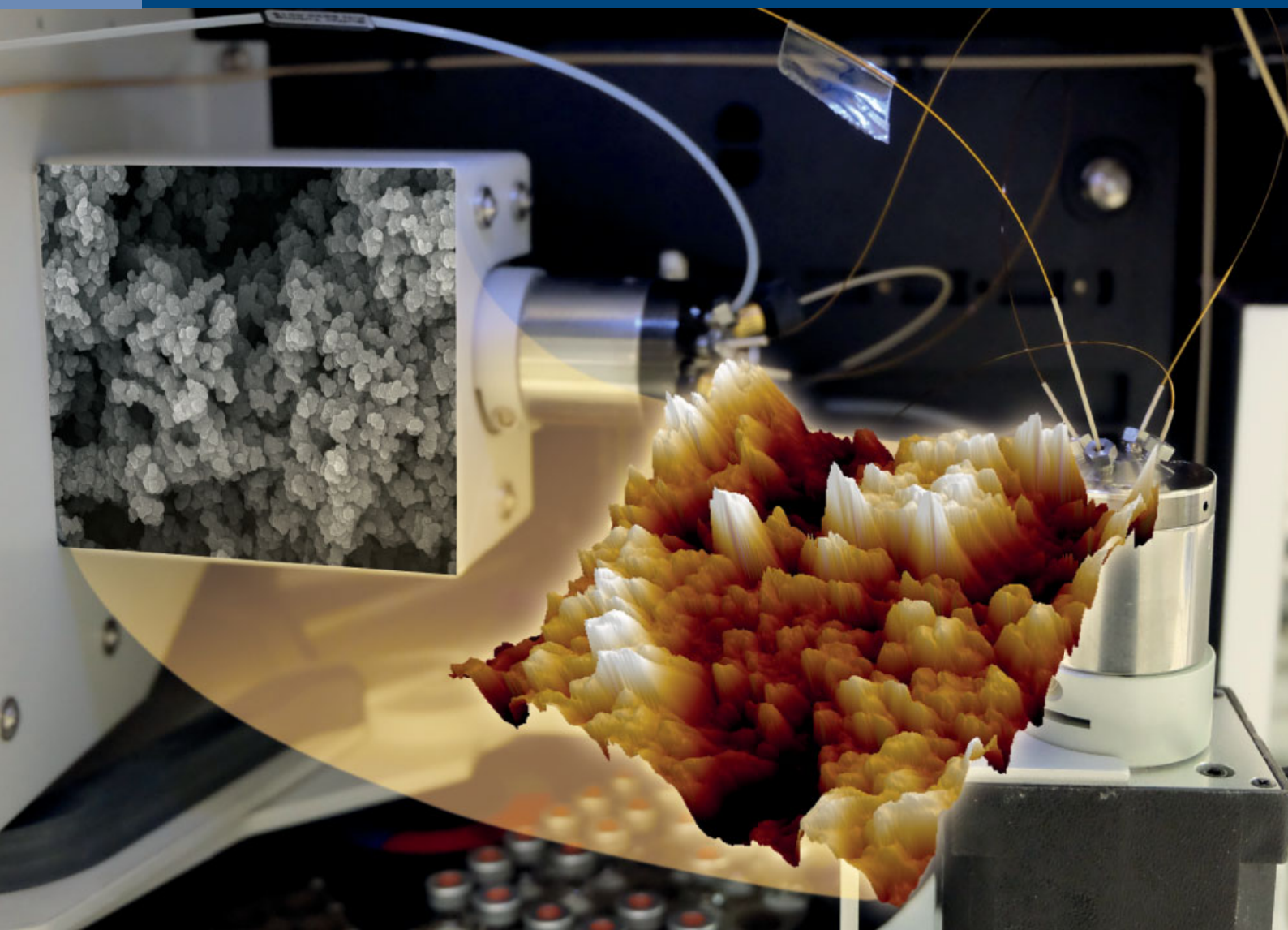
It is not permitted to download or to forward/distribute the text or part of it without the consent of the author(s) and/or copyright holder(s), other than for strictly personal, individual use, unless the work is under an open content license (like Creative Commons).

#### Disclaimer/Complaints regulations

If you believe that digital publication of certain material infringes any of your rights or (privacy) interests, please let the Library know, stating your reasons. In case of a legitimate complaint, the Library will make the material inaccessible and/or remove it from the website. Please Ask the Library: <https://uba.uva.nl/en/contact>, or a letter to: Library of the University of Amsterdam, Secretariat, Postbox 191, 1000 GD Amsterdam, The Netherlands. You will be contacted as soon as possible.

JOURNAL OF  
SEPARATION  
SCIENCE

23 | 16



**Methods**  
Chromatography · Electroseparation

**Applications**  
Biomedicine · Foods · Environment

[www.jss-journal.com](http://www.jss-journal.com)

WILEY-VCH

Sam Wouters<sup>1</sup>  
 Tom Hauffman<sup>2</sup>  
 Marjo C. Mittelmeijer-  
 Hazeleger<sup>3</sup>  
 Gadi Rothenberg<sup>3</sup>  
 Gert Desmet<sup>1</sup>  
 Gino V. Baron<sup>1</sup>  
 Sebastiaan Eeltink<sup>1</sup>

<sup>1</sup>Vrije Universiteit Brussel,  
 Department of Chemical  
 Engineering, Brussels, Belgium

<sup>2</sup>Vrije Universiteit Brussel,  
 Department of Materials and  
 Chemistry, Research group of  
 Electrochemical and Surface  
 Engineering, Brussels, Belgium

<sup>3</sup>University of Amsterdam, Van 't  
 Hoff Institute for Molecular  
 Sciences, Amsterdam, The  
 Netherlands

Received August 9, 2016  
 Revised September 27, 2016  
 Accepted September 27, 2016

## Research Article

# Comprehensive study of the macropore and mesopore size distributions in polymer monoliths using complementary physical characterization techniques and liquid chromatography

Poly(styrene-co-divinylbenzene) monolithic stationary phases with two different domain sizes were synthesized by a thermally initiated free-radical copolymerization in capillary columns. The morphology was investigated at the meso- and macroscopic level using complementary physical characterization techniques aiming at better understanding the effect of column structure on separation performance. Varying the porogenic solvent ratio yielded materials with a mode pore size of 200 nm and 1.5  $\mu\text{m}$ , respectively. Subsequently, nano-liquid chromatography experiments were performed on 200  $\mu\text{m}$  id  $\times$  200 mm columns using unretained markers, linking structure inhomogeneity to eddy dispersion. Although small-domain-size monoliths feature a relatively narrow macropore-size distribution, their homogeneity is compromised by the presence of a small number of large macropores, which induces a significant eddy-dispersion contribution to band broadening. The small-domain size monolith also has a relatively steep mass-transfer term, compared to a monolith containing larger globules and macropores. Structural inhomogeneity was also studied at the mesoscopic level using gas-adsorption techniques combined with the non-local-density-function-theory. This model allows to accurately determine the mesopore properties in the dry state. The styrene-based monolith with small domain size has a distinctive trimodal mesopore distribution with pores of 5, 15, and 25 nm, whereas the monolith with larger feature sizes only contains mesopores around 5 nm in size.

**Keywords:** Adsorption isotherms / Column characterization / Gel porosity / Porosimetry / Stationary phases  
 DOI 10.1002/jssc.201600896



Additional supporting information may be found in the online version of this article at the publisher's web-site

## 1 Introduction

Rigid polymer-monolithic stationary phases for LC were introduced in the early 1990's as an alternative for columns packed with spherical particles [1]. Monoliths feature a macroporous interconnected network structure of clustered polymer globules. Similar to the relation between particle size and separation efficiency ( $H_{min} = f(d_p)$ ) of particle-packed

columns [2], the kinetic separation performance of polymer-monolithic stationary phases is primarily dictated by the domain size, i.e., the sum of the macropore size and the size of the polymer microglobules [3]. Indeed, decreasing the size of the macropores and microglobules by adjusting the composition of the polymerization precursor mixture (e.g., changing the porogen composition, or the monomer-to-porogen ratio) or altering the polymerization reaction conditions (such as the polymerization temperature and time), can enhance the separation efficiency [4–7].

Despite the relatively heterogeneous macropore structure of polymer monoliths, which enhances eddy dispersion (negatively affecting efficiency) [8], polymer-monolithic columns were successfully applied for the gradient separation of biomolecules including intact proteins and their isoforms [9, 10], DNA [11], peptides [12], and also synthetic polymers [13, 14]. This good kinetic performance, however, contrasts with the efficiency reported for small-molecule

**Correspondence:** Dr. Sebastiaan Eeltink, Pleinlaan 2, B-1050, Brussels, Belgium  
**E-mail:** seeltink@vub.ac.be  
**Fax:** +32-0-2-629-3248

**Abbreviations:** AFM, Atomic-force microscopy; BET, Brunauer–Emmett–Teller; IUPAC, International Union of Pure and Applied Chemistry; MIP, Mercury-intrusion porosimetry; NLDFT, Non-local density function theory; PSD, Pore size distribution

separations [15, 16]. Significant chromatographic dispersion was attributed to the ability of small molecules to penetrate the meso- and micropores of the stationary phase and to surface-diffusion effects [17, 18]. Penetration of small molecule solutes in the polymer globules, facilitated by swelling induced by the use of a high content of organic modifier in the mobile phase, which can affect the resulting peak width and hence separation efficiency [8].

IUPAC defines mesopores to range from 2 to 50 nm, with sub-2 nm pores being classified as micropores, and pores larger than 50 nm to be macropores. To understand the relation between the monolithic pore structure and dispersion of small and large molecules, more detailed information is required about the micro-, meso-, and macropore distributions. Physical characterization techniques such as scanning-electron microscopy and mercury-intrusion porosimetry (MIP) have been frequently applied to characterize respectively the microglobule size and the macropore size distributions in the dry state, respectively [19, 20]. Macropore sizes obtained from MIP data are generally in good agreement with those derived from inverse size-exclusion chromatography experiments [21]. As an alternative to MIP to study the mesoporosity of porous materials, mesopore analysis of such materials is typically performed using gas-adsorption techniques [22]. Modeling of the adsorption-desorption data allows to establish pore-size distributions in the meso- and micropore range. However, recent studies demonstrated that the conventionally used pore models based on the Kelvin equation such as the Barrett–Joyner–Halenda model, the Horvath–Kawazoe model, and the Saito–Foley model, do not take into account physical phenomena arising in materials that exhibit both micro- and mesopores [23]. The contributions in the isotherms caused by phenomena such as tensile-strength and pore-network effects, adsorbate phase transitions, and monolayer formation, often lead to an underestimation of the true pore size [24]. Alternatively, one can use the non-local density function theory, which is based on molecular simulations and molecular dynamics [25]. Most recently, this approach was adopted by IUPAC [26]. Recently, we addressed the properties of the materials under realistic experimental conditions (*e.g.*, wetted state), by an NMR spectroscopy study of a polymer monolith wetted with acetonitrile. The results revealed the presence of acetonitrile with restricted mobility, likely to be present in the confines of micro- and mesopores, and adsorbed to the surface [27]. To characterize this swelling behavior in the presence of typical reversed-phase solvents such as water and acetonitrile, an atomic force microscopy (AFM) study was reported by Laher *et al.* [28]. There, the monolith was embedded in a resin followed by longitudinal microtoming, allowing to probe the surface of cross-sectioned globules, but possibly not the true surface of the polymer globules. Also, in this configuration the material is restricted to axial swelling, not having its usual degrees of dimensional freedom.

In recent years, TEM [29] and block-face SEM have been used to characterize the macropore structure of monolithic

stationary phases. The latter technique was used to create three-dimensional reconstructions (typically with dimensions in the order of  $40 \times 40 \times 40 \mu\text{m}^3$ ) of monolithic materials by means of analyzing hundreds of 50 nm thick cross-sections. In this way both monolithic disks [30–32], as well as monoliths prepared in a capillary column format were analyzed [33–35]. Simulation of flow inside these monolithic entities has allowed to establish a better understanding of the relation between porous properties and morphology of polymer monoliths, and mass transport and dispersion characteristics in these materials. For example, Jungbauer *et al.* [32] could relate the permeability of polymer monoliths to alternating channel width and interconnectivity of narrow and wide pores. The existence of preferential flow paths, entrapment of probes at constrictions and dislodgement of these probes by diffusion was also demonstrated using these modeling approaches, accounting for the influence of flow rate on these phenomena [31].

The present study reports on the synthesis and the characterization of the morphology of polymer monoliths on the macro-, meso-, and micropore levels using SEM, MIP, and gas-adsorption experiments (with different gasses and operating ranges to study possible swelling behavior). Possibilities and limitations of the techniques are discussed. The results of the physicochemical study are complemented with chromatographic experiments using un-retained tracers to correlate apparent structural inhomogeneity to flow transport behavior and dispersion characteristics. Results are presented for two types of poly(styrene-*co*-divinylbenzene) monoliths featuring different porous properties. To probe the swelling behavior of the stationary-phase surface under wetting conditions, atomic-force microscopy experiments were conducted in a controlled liquid environment.

## 2 Materials and methods

### 2.1 Materials and chemicals

Acetonitrile (ACN, LC–MS grade), 2,2'-azobisisobutyronitrile (AIBN, 98%), 1-decanol (99%), methanol (chromasolv, 99.5%), potassium iodide (KI, 99%), tetrahydrofuran (THF, anhydrous, without stabilizer, 99.9%), toluene (anhydrous, 99.8%), 3-(trimethoxysilyl)propyl methacrylate (98%) and uracil (99%) were purchased from Sigma–Aldrich (Bornem, Belgium). Styrene (S, 99.5%), divinylbenzene (DVB, technical, 65% mixture of *m*-DVB and *p*-DVB, 35% ethylvinylbenzene), and sodium hydroxide pellets were purchased from Merck (Hohenbrunn, Germany). Hydrochloric acid (30 vol %) was purchased from Fluka (Buchs, Germany). S and DVB were purified over activated alumina columns to remove inhibitor, all other products were used as received. Water was purified using a MilliQ system (Merck Millipore, Darmstadt, Germany). Poly(imide)-coated fused-silica tubing (200  $\mu\text{m}$  id  $\times$  360  $\mu\text{m}$  o.d.) was purchased from Polymicro Technologies (Molex, Lisle, USA).

**Table 1.** Polymerization mixture compositions in weight percentage for the preparation of the poly(styrene-*co*-divinylbenzene) monolithic materials

wt% S	wt% DVB	wt% THF	wt% 1-decanol	wt% AIBN*
15.0	15.0	17.5	52.5	3.0
15.0	15.0	14.0	56.0	3.0

\*Percentage of AIBN initiator relatively to mass of monomers.

## 2.2 Monolith synthesis

Capillary fused-silica tubing was pretreated to establish covalent bonding of the polymer monolith to the column inner wall using a surface modification procedure described in literature [36]. In summary, the surface was activated by flushing columns with 1 M NaOH solution (30 min, 2  $\mu$ L/min) and subsequent flushing with 1 M HCl (30 min, 2  $\mu$ L/min). The columns were then functionalized by flushing with (trimethoxysilyl)propyl methacrylate (10 vol% in toluene, 60 min, 2  $\mu$ L/min). After each of the three steps, the capillaries were emptied and dried with pressurized air. The pretreated capillaries were stored in a desiccator.

Table 1 lists the compositions of the polymerization mixtures used in this study. The reaction mixtures were stirred for 10 min and subsequently degassed in an ice-cooled ultrasonic bath for 10 min. The polymerization mixture was introduced in the pretreated fused-silica capillary, sealed with septa, and placed in a thermostatted water bath (Julabo, Seelbach, Germany) at 70°C. After 24 h of reaction, the monolithic columns were flushed with methanol using an HPLC pump. Each column was prepared in duplicate. Monolithic materials were also prepared in bulk quantity using 2 mL sample vials. After completion of the polymerization reaction, the glass vials were carefully broken to remove the monolithic materials. The intact monolithic rods were then subjected to Soxhlet extraction with methanol for 24 h and dried in a desiccator. For measurements requiring the use of bulk samples, these were first carefully fragmented into smaller pieces to fit the sample holders and to minimize “skin” effects, which were noted to have an important effect otherwise (*i.e.*, a 7–10% smaller pore volume was recorded when not fragmented).

## 2.3 Characterization

A JSM-6400 scanning-electron microscope (JEOL, Tokyo, Japan) was used to obtain micrographs of cross-sections of capillary monolithic columns. Samples were sputtered with a 6 nm layer of Pt-Pd to reduce charging of the polymer-monolithic material. The instrument was operated at acceleration voltages of 20 keV in secondary-electron-imaging mode (SEM-SEI).

Atomic-force microscopy (XE 100, Park Systems, Suwon, S. Korea) was used to map the surface topology of the polymer microglobules. Measurements were performed in non-contact mode applying constant force and a scan rate

corresponding to 2  $\mu$ m/s. This mode was selected not to induce any lateral forces on the surface of the globules. N-type Si tips with Al coating (ACTA tips, AppNano, Mountain view, USA) were used, having an average tip radius of 10 nm. The topographical images were corrected with a first order flattening procedure. XEI software (Park Systems) was used for data treatment. Measurements were performed on cross-sections of monoliths synthesized in capillary tubing. Tubing was sectioned using a ceramic blade and fixed in a custom-made Teflon sample holder. To study the material under wetting conditions, the sample was submerged by pouring liquid into the sample holder. Line profiles were used to estimate the average size of the globules.

Gas-adsorption experiments were run on a Quantasorb Autosorb AS-1 (Quantachrome Instruments, Boynton Beach, USA). The use of bulk samples was required to have sufficient adsorbate mass, given the low specific weight of polymer monoliths. Samples were activated at 393 K and subjected to sorption experiments with argon at 87.5 K. Argon is preferably used over nitrogen for accurate measurement of micropores, as adsorption of the larger N<sub>2</sub> in micropores occurs at lower  $P/P_0$  values than Ar [24]. Adsorption-branch data was processed using the multi-point Brunauer–Emmett–Teller (BET) model (Langmuir-based multilayer gas adsorption model, modern Rouquerol method) [37] and using the non-local density function theory (NLDFT) method designed for zeolites/silica with cylindrical pores [38], which provided the best fit (smallest fitting errors) for the polymer monoliths. Nitrogen-adsorption experiments were performed at 77 K (after activation at 393 K) to verify the results.

Bulk samples were also subjected to mercury-intrusion porosimetry using Pascal 140 and 440 mercury-intrusion porosimeters (CE Instruments, Milan, Italy) for low- and high-pressure analysis, respectively. Data was treated with the Washburn equation [39] considering cylindrical pores, a surface tension of 0.48 N/m for mercury, and a 140° contact angle of mercury with the sample surface.

Isocratic nanoLC experiments were performed using an Ultimate 3000 RSLCnano system (Thermo Fisher Scientific, Germering, Germany) equipped with a 4 nL injection valve (Valco, Schenkon, Switzerland). The 200 mm column was mounted directly on the valve and connected to the inlet capillary (30  $\mu$ m id  $\times$  150 mm) of the detector using a Nano connector sleeve (Thermo Fisher Scientific). UV detection was performed using a 3 nL flow cell at  $\lambda = 254$  nm using 10 Hz data collection rate and 0.2 s response time. Results are based on triplicate injections of unretained markers. Chromeleon (version 6.80, SR11) was used for instrument control, processing, and data management.

## 3 Results and discussion

### 3.1 Morphology at the macroscopic level

The morphology of poly(styrene-*co*-divinylbenzene) monoliths was tuned by optimizing the composition of the

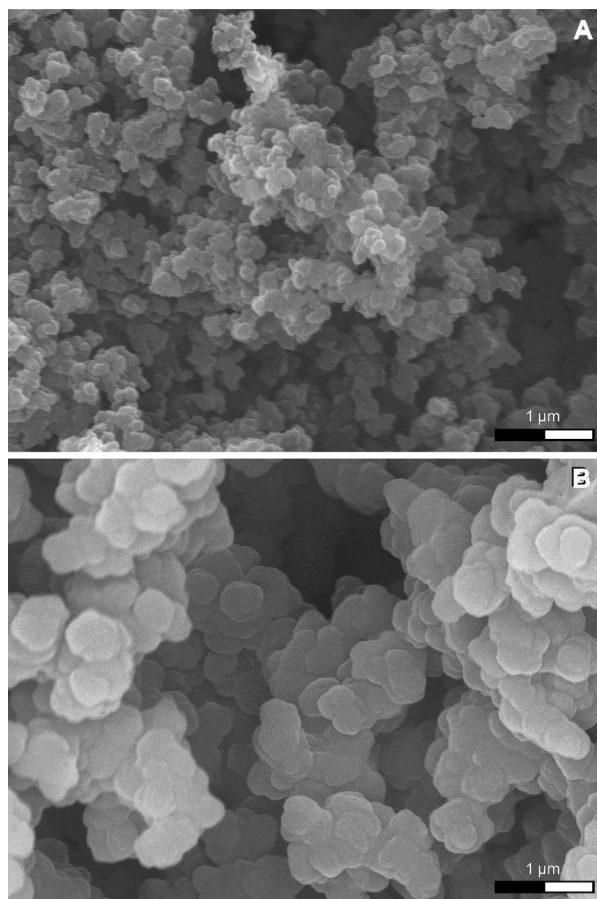


**Figure 1.** Scanning electron micrographs of the cross-sections of fused-silica capillary monolithic columns obtained by secondary-electron imaging of poly(S-co-DVB) monoliths synthesized with (A) 17.5 wt% and (B) 14.0 wt% of THF.

binary pore-forming solvent-system, i.e., THF and 1-decanol. The porogens are selected based on solubility parameters to yield a homogenous precursor mixture and a solvent combination in which one solvent is prone to swelling the polymer material being formed ('good' solvent), and the other solvent is prone to induce phase separation ('poor' solvent) during synthesis. Figure 1 shows scanning electron micrographs of the resulting macroporous materials prepared in situ in 200  $\mu\text{m}$  id capillary column format, featuring submicron globules. These micrographs can be used to provide an estimate for the mode diameter: 150 (A) and 400 nm (B), respectively. By increasing the amount of 'good' solvent (THF) in the porogen, the reaction-induced phase separation is postponed [40], and the solvent-to-monomer ratio in the growing microglobules/microgel and surrounding 'sol' during polymerization is altered, which in turn leads to the formation of a larger number of smaller globules. For exact compositions see Table I, materials and methods. In the Supporting Information Fig. S1, a comparison is made between the morphologies of monoliths synthesized in capillary format and in bulk, the latter being used for mercury-intrusion porosimetry and gas-adsorption experiments. Although similar domain sizes

are observed, Byrström et al. discussed that the variations in porous structure induced by differences in mold size may not be evidently visible [41].

### 3.2 Homogeneity of the macropore structure and its relation to eddy dispersion

To study the porosity and pore-size distributions (PSD) of these materials, mercury-intrusion porosimetry (MIP) was performed on bulk samples (see Fig. 2). The cumulative pore-volume curve  $D_0$  (where  $D_0(D_i) = V_{cum}(D_i) = \sum_i \Delta V_i$ ) decreases with increasing pore diameter because the largest pores are filled first (oppositely to what is taking place during gas-adsorption experiments) and the sum of all pore-volume increments represents the total pore volume. The monolithic material with smaller domain sizes features a lower cumulative pore volume, while the content of monomers and porogen were kept constant during synthesis, which should in principle yield identical total porosity after 24 h polymerization time yielding full conversion [40]. This may imply that these materials exhibit porosity outside the pore range studied with MIP, which is limited to studying the macropore domain, as sensitivity in the range of the mesopores is considered lower compared to gas adsorption techniques. Various visualization approaches exist to represent pore-size distributions, some of which may overemphasize larger pores in multimodal pore systems [42]. In Fig. 2A and 2B the differential pore-volume distribution  $D_2$  or pore-volume density ( $dV/dD$  where  $D_2(D_i) = \Delta V_i/\Delta D_i$ ) is plotted as function of pore diameter. The normalization accounts for irregular data-point spacing, enabling a direct comparison of the PSD of different materials over the entire range of pore-diameter values, as recommended by IUPAC [43]. Another commonly used representation in logarithmic scales can be found in the Supporting Information Fig. S2. By using a linear pore-diameter scale representation however, the area under the curve in a given pore-size range is directly proportional to the pore volume. It should be noted that a large pore volume in the small-pore diameter range is the contribution of a large number of pores, and vice versa, i.e., a large pore volume in the large-pore diameter range is the result of a small number of such pores. Figure 2A shows that the small domain-size monolith exhibits a pore-size distribution with the vast majority of macropores in a narrow range between 150 and 300 nm. The large domain-size monolith features a broad PSD with macropores ranging between 500 nm and 3  $\mu\text{m}$  (Fig. 2B). Two acrylate monolithic materials with different porous properties were also studied and a similar behavior was noted during MIP analysis (see Supporting Information Figs. S6 and Fig. S7 for the respective SEM and MIP results). The alternative representation of the data as shown in Fig. 2C is obtained by normalizing the ordinate to the mode pore size,  $D_{mode}$ , corresponding to the maximum value of the  $dV/dD$  signal for each sample. The abscissa is normalized by multiplying  $dV/dD$  by  $D_{mode}$  divided by the total volume,  $V_{tot}$ . Figure 2C shows that the small-domain monolith with a relatively narrow

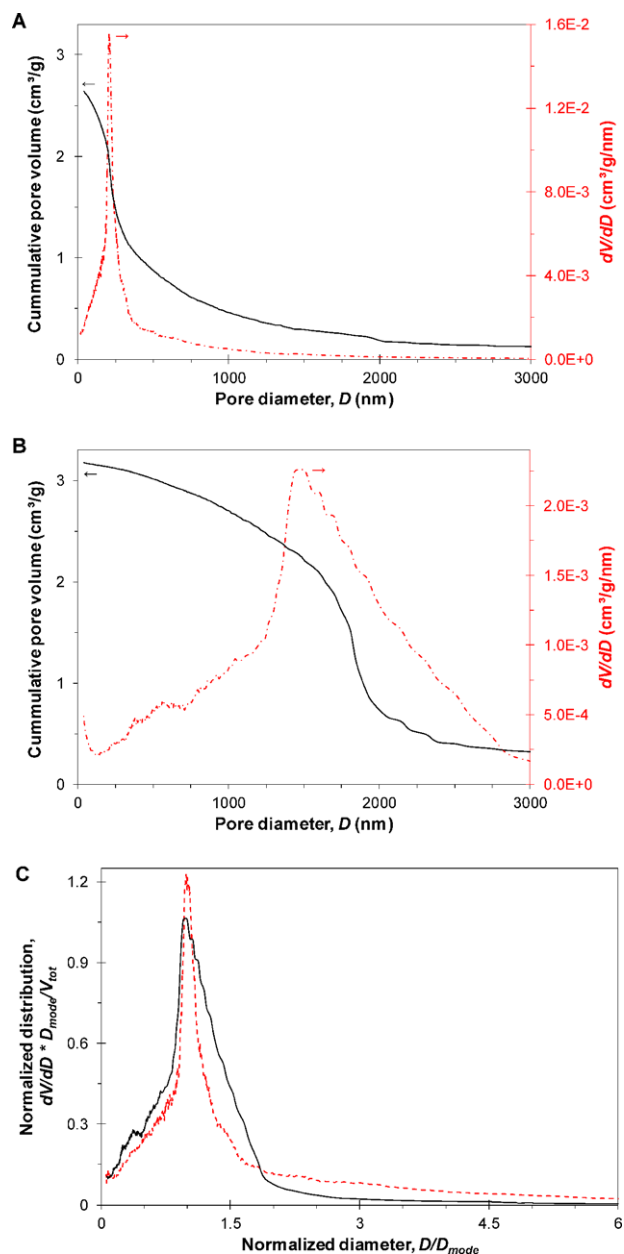


**Figure 2.** Mercury-intrusion porosimetry data for bulk samples of poly(S-co-DVB). Pore diameter is plotted on a linear scale as a function of the cumulative pore volume  $D_0$  (solid line) and pore size distribution  $D_2$  (dash-dotted line) for monoliths synthesized with (A) 17.5 wt% and (B) 14.0 wt% of THF. An alternative normalized or reduced representation of the data (C) for the materials synthesized with 17.5 wt% (dash-dotted line) 14.0 wt% of THF (solid line).

distribution closely centered on the mode pore diameter also exhibits a long tail of large pores. The pore-size distribution of the large-domain size monolith is slightly broader, but this monolith does not feature such a ‘tail’.

The PSD of monolithic stationary phases were also compared with that of a particle-packed column, by performing an MIP experiment in which 5  $\mu\text{m}$  fully porous stationary phase (Hypersil) beads were introduced in the sample holder, see

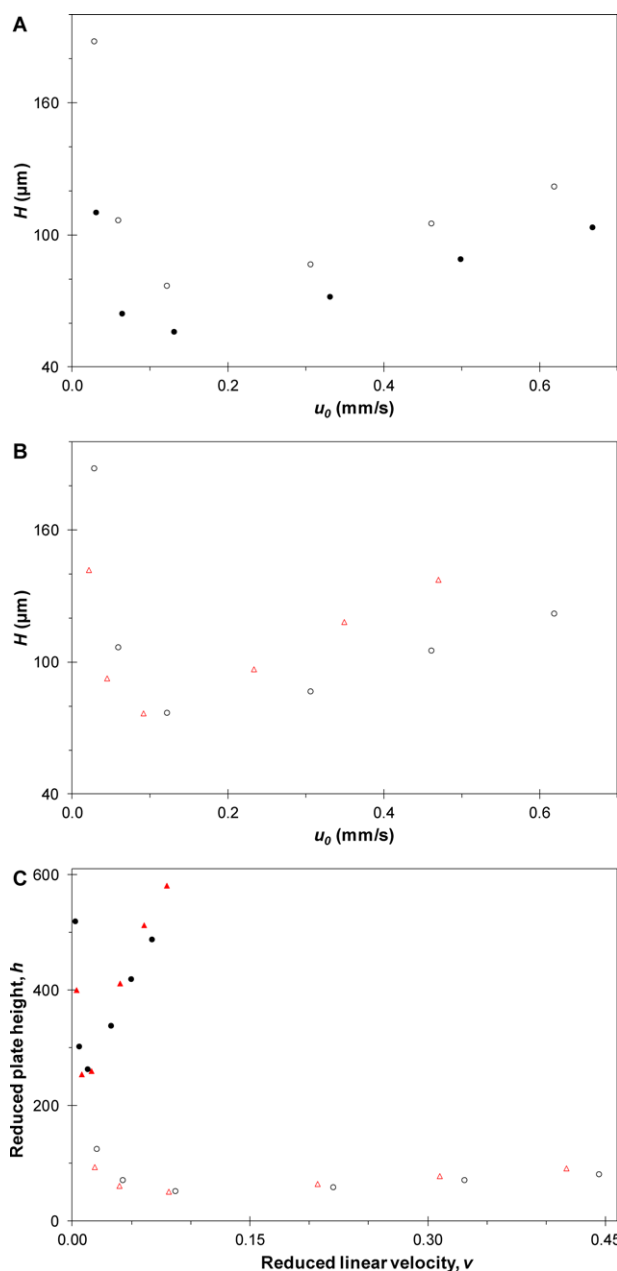


**Figure 3.** Isocratic nano-liquid-chromatography experiments on  $0.2 \times 200$  mm poly(S-co-DVB) monolithic columns. (A) van Deemter plots recorded for KI while applying pure water on a column synthesized with 17.5 wt% (●) and 14.0 wt% of THF (○). (B) van Deemter plots recorded on a column synthesized with 14.0 wt% of THF for uracil ( $\Delta$ ) while applying 75:25 v/v(%) ACN:H<sub>2</sub>O and KI (○) while applying pure water (C) Reduced van Deemter curves for recorded on monoliths synthesized with 17.5 wt% (KI ●, uracil  $\blacktriangle$ ) and 14.0 wt% of THF (KI ○, uracil  $\triangle$ ). Results based on triplicate injections.

Supporting Information Fig. S3. This approach would mimic “dry-packing conditions” which has previously been used to pack columns with large 10–20  $\mu\text{m}$  particles [44]. Currently, high-pressure slurry packing is the technique of choice to create high-efficiency columns yielding higher packing density, but this approach is not compatible with the MIP sample

holder. Therefore, Supporting Information Fig. S3 only provides a rough estimation (and likely overestimation) of the PSD of current state-of-the-art packed column technology. Still, this experiment reveals that the PSD of packed beds (for this type of stationary phase) is in the same range as the large-domain size polymer monolith.

The presence of structural inhomogeneity in monoliths induces eddy dispersion (A-term contribution to band broadening) and instead of having a well-defined narrow velocity profile in the column, a heterogeneous flow profile is formed characterized by a broad range of flow velocities. To characterize the magnitude of eddy dispersion, isocratic nano-liquid-chromatography experiments were conducted to determine the plate height of different unretained markers (KI and uracil) as a function of flow rate (50 nL/min to 1  $\mu$ L/min). To minimize extra column band-broadening effects, the capillary column was directly mounted on the 4 nL injection valve and UV detection was performed employing a 3 nL UV flow cell. Plate heights ( $H$ ) were calculated based triplicate measurements and recording the peak width at half height and the  $t_0$  time. Figure 3A shows the resulting plate-height curves ( $H$  versus  $u_0$ ) using KI as the  $t_0$  marker and applying water as the mobile phase. When comparing the minimum plate-height values ( $H_{min}$ ) of the small- and large-domain-size monoliths, it is evident (and expected) that the small domain-size monolith performs better in terms of separation efficiency. To account for a possible swelling effect, nanoLC experiments were also conducted applying 75:25 v/v ACN/H<sub>2</sub>O as the mobile phase and injecting uracil as the  $t_0$  marker. The pressure drop normalized for the viscosity indicated the presence of a swelling effect at higher ACN concentration. Figure 3B shows an overall increase in C-term contribution for the large-domain size monolith when applying 75:25 v/v ACN/H<sub>2</sub>O instead of water as the mobile phase (a similar trend was noted for the small-domain size monolith, data not shown). Swelling would effectively decrease the size of the pores (slightly decreasing the  $C_m$ -term contribution), but also increases the globule size and hence amplifies the  $C_s$ -term contribution.

When normalizing  $H$  and  $u_0$  based on the mode pore size as determined with MIP, the reduced plate-height curves ( $h$  versus  $\nu$ ) depicted in Fig. 3C are obtained. In case of self-similar structures (such as columns packed with different particle size) the reduced van Deemter curves should yield a perfect overlay [45]. However, this representation shows that the large-domain size monolithic column outperforms the column with smaller domain size. Apparently, the presence of (even a small number) of large (> 1  $\mu$ m) macropores in the small-domain size monolithic column, significantly disrupts the flow profile, and leads to a relative large A-term contribution. Furthermore, a steep increase in plate height in the C-term region of the van Deemter curve is noted, in case of the small-domain size monolith. This may reflect the presence of a relative large mobile-phase mass-transfer ( $C_m$ -term) contribution caused by larger diffusion distance towards the stationary-phase surface in combination with the presence of a parabolic flow profile in these “relatively large” macropores.

Also, since the small domain-size monolith contains relatively more mesopores than the monolithic materials featuring larger macropores and globules, the  $C_s$ -term may be enhanced (see Section 3.3). These hypotheses can be corroborated when taking into account conclusions of flow simulations in a reconstructed monolithic entity by Lenhoff et al., who reported extensive heterogeneity of flow and that the flow field is skewed toward lower velocities [30]. Using a similar approach, Tallarek et al. also reported the existence of large pores in a P(S-co-DVB) monolithic material prepared in capillary format [33]. Lee et al. also concluded that a reduction in feature sizes in a capillary monolith resulted in increased heterogeneity, compromising the expected positive on column performance [35].

When normalizing the  $H$  and  $u_0$  based on the mode pore diameter it is noted that the minimum of the van Deemter curve is situated at a very low reduced velocity. This is likely caused by an underestimation of the “characteristic size”. However, when normalizing the plate height and mobile-phase velocity based on either globule size or domain size (data not shown) the same trends were obtained.

The physical characterization techniques utilized are useful to study polymer monoliths, with the limitation that the experiments are performed in the dry state, while these materials are used in practice in the solvated state. In an attempt to probe the swelling behavior of polymer monoliths at the macroscopic level under solvated conditions, atomic-force-microscopy measurements were conducted both in the dry state and in wetted state applying acetonitrile (typically used for RP-LC). In an experiment previously reported, shrinkage of globules of an acrylate cation-exchange monolith was observed when wetted with water [46]. A swelling effect is however expected when solvating with an organic eluent. The measurements in the dry state (Fig. 4A) provide a topological image that is consistent with the observations using the complementary characterization techniques presented in this work. Starting from the contour plots and applying a line scan, which provides a height profile along the line, it can be observed that globule sizes in wetted condition (Fig. 4C) are larger compared to the data obtained in dry state (Fig. 4B), which shows that swelling is taking place in the presence of organic solvent. This swelling effect will affect the macroporosity of the material to some extent. Similar to Skinner et al., [46] we were unable to resolve any mesoporous features or alterations to the actual surface using AFM under wetting conditions.

### 3.3 Mesopore characterization using gas-adsorption techniques

To characterize the monolithic mesopore and micropore structure, adsorption-desorption isotherms were recorded using argon at 87 K. The comparison of the adsorption-desorption isotherms for the two poly(S-co-DVB) monolithic materials is shown in Fig. 5A. A large hysteresis between adsorption and desorption of the gas is noted over

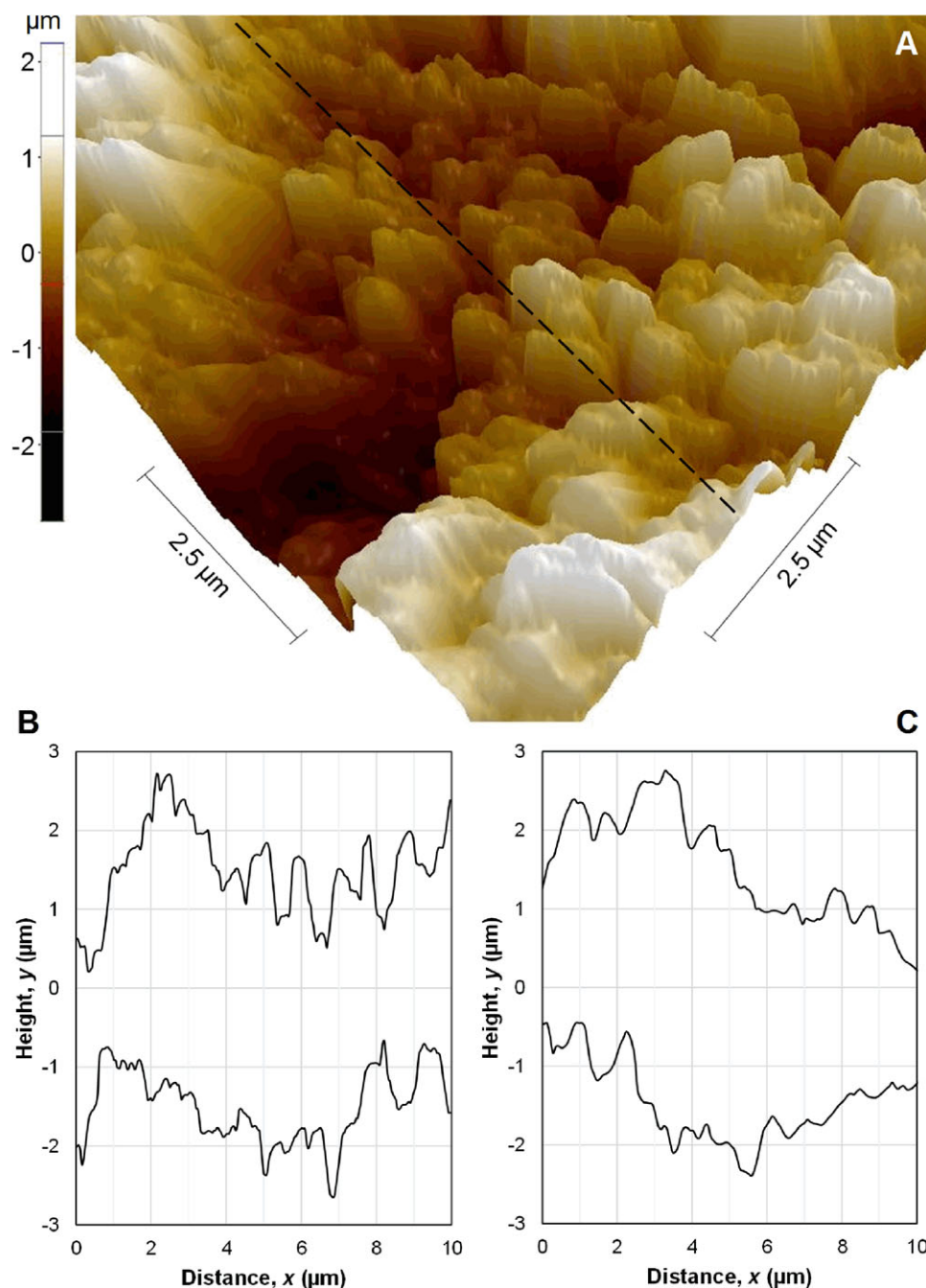


**Figure 4.** (A) Topography of a P(S-co-DVB) monolith synthesized with 14.0 wt% of THF (see Fig. 1B) recorded on the cross-section of a capillary by means of atomic-force microscopy in the dry state. The dashed line indicates a possible line scanning position. (B) Representative line-scans in the dry state (providing a height profile when scanning in the x direction). (C) Representative line scans wetted with acetonitrile. Data have been shifted for the sake of clarity.

a broad range of relative pressures. At low relative pressures ( $P/P_0 < 0.02$ ), the adsorbate is again released, leaving the material in an unaltered form with identical behavior as recorded in subsequent measurements. The hysteresis is induced by dissolving of the adsorbate into the polymer material, which results in swelling of the monolithic material. A similar but smaller hysteresis was observed for acrylate monoliths with different porous properties (Supporting Information, Fig. S8). In a control experiment using nitrogen at 77 K similar adsorption-desorption hysteresis over the broad  $P/P_0$  was recorded for the styrene-based monolith, albeit a less open one (Supporting Information Fig. S4) and an 8% smaller

pore volume and surface area was recorded. Nitrogen is larger than argon and thus considered less sensitive when analyzing micropores. Furthermore, the nitrogen adsorption-desorption experiments are conducted at lower temperature, which may affect the rigidity of the polymer matrix (and hence the extent of swelling). In an additional ‘scanning’ experiment on the styrene monolith, the adsorption was carried out up to relative pressures of 0.75, 0.50, and 0.10, respectively (Supporting Information, Fig. S5). Similar adsorption-desorption behavior is observed, albeit with a smaller hysteresis, reflecting the narrower  $P/P_0$  range scanned and adsorbate mass reached. This indicates that the polymer

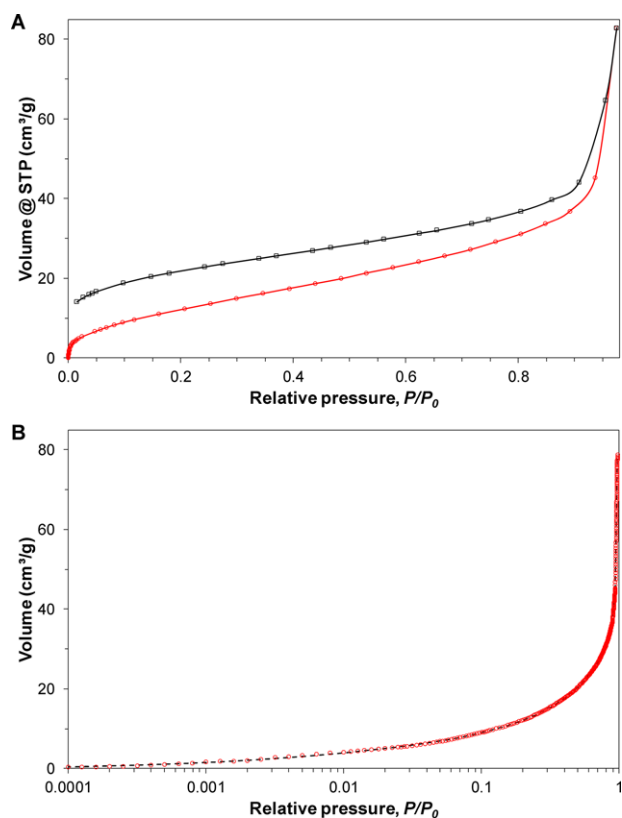


**Figure 5.** (A) Argon adsorption (○) and desorption isotherms (□) and (B) illustration of a NLDFT fit (solid line) of the measured adsorption data (○) for a bulk P(S-co-DVB) monolith synthesized with 17.5 wt% of THF.

material swells gradually, independent of the absolute pressure applied.

A multi-point BET analysis of the data showed that the monolith with smaller domain size has a 5.7-fold higher surface area, *i.e.*, 44.25 m<sup>2</sup>/g ( $R^2 = 0.9998$ ) for the small domain monolith and 7.81 m<sup>2</sup>/g ( $R^2 = 0.9997$ ) for the large-domain monolith. The pore volume was determined applying the non-local-density function theory (NLDFT) modes to fit the experimental data measuring during adsorption (Fig. 5B). The best model fit was obtained applying a model developed for silica/zeolites exhibiting cylindrical pores. Fitting errors (least square fitting) ranged only between 0.66–1.26% for the different polymer-monolithic materials. Larger fitting errors were obtained when using nitrogen, or when using different pore models. The resulting pore-size distributions are shown in Fig. 6A and B. The cumulative volume of the micro/mesopores of the small-domain monolith is eightfold higher compared to the monolith with larger macropores and globules. This is in agreement with the results from the MIP experiments, where a smaller pore volume was recorded for the monolith with a small feature size. Moreover, the hysteresis is larger for monoliths with smaller domain size, thus, the uptake and capture of argon inside the material is larger. This can be explained by considering that this monolith exhibits a larger surface-to-volume ratio, as confirmed by

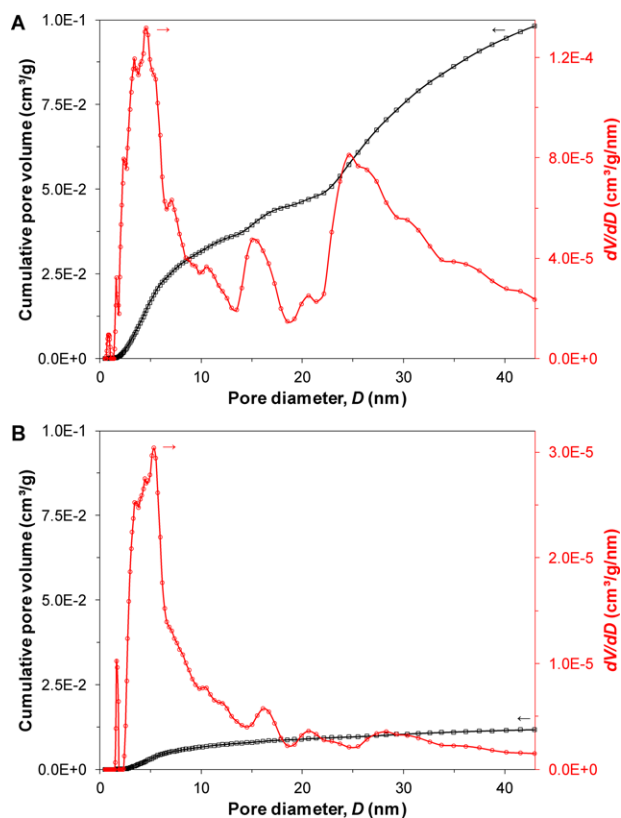


**Figure 6.** NLDFT-analysis results of argon-adsorption measurements on bulk samples of P(S-co-DVB). Pore diameter is plotted on a linear scale as a function of the cumulative pore volume  $D_0$  (□) and pore size distribution  $D_2$  (○) for monoliths synthesized with (A) 17.5 wt% and (B) 14.0 wt% of THF.

BET, and that argon can only penetrate the outer surface of the globules. A contributor to this effect is the copolymerization composition drift formed during the free-radical copolymerization, which induces a gradient in crosslink density in the globules (outer surface is less crosslinked and thus more prone to swelling) [38, 47]. Also notable is that the styrene-based monolith with small domain size has a distinctive trimodal pore distribution (Fig. 6A), whereas the monolith with larger feature sizes, only contains pores around 5 nm in size (Fig. 6B). The 15 and 25 nm pores present in the small-domain monolith are likely to be formed during clustering or agglomeration of the small microglobules during the formation of the polymer monolith, as noticed also for the acrylate system (Supporting Information Fig. S8).

## 4 Concluding remarks

Information on the relation between morphology and separation performance can be used to optimize shape and porosity of future chromatographic materials. Polymer-monolithic materials can potentially outperform packed columns, since the macropore size and globule size can be tuned independently from the total porosity (by optimizing the composition

of the precursor mixture [5]), whereas for packed-bed columns the efficiency is related to particle size, but the total external porosity is fixed. However, one of the key parameters is also to control the structure homogeneity, which affects eddy dispersion. This study showed that with conventional thermally induced free-radical polymerization, it currently seems impossible to create self-similar monolithic structures when reducing the macropore/globule size. As a result, one cannot readily predict gain factors in efficiency and/or analysis time that may be achieved when creating much smaller monolithic nanostructures (as can be done with packed columns and kinetic theory [48]).

Information on the mesoscopic pore structure may ultimately lead to the elucidation of mass-transfer band-broadening effects noted for small-molecules separation [17, 27]. Gas-adsorption isotherms provide accurate information on the mesopores size distribution (in dry state), provided that the NLDFT model is applied. Experiments demonstrated that the outer surface of the polymer microglobules is prone to swelling (dry-state experiment), which greatly affects the desorption isotherm. It should be noted that in chromatographic experiments, the use of wetting and dewetting solvents affects swelling of the polymeric globular surface, which further complicates probing the relation between macro- and mesoscopic structure on separation performance.

*Support of this work by grants of the Flemish Agency of Innovation and Entrepreneurship (VLAIO) and the Research Foundation Flanders (FWO 1508914N, 1517517N, and G025916N) are gratefully acknowledged. José Luís Soares-Sousa and Priya Laha (Vrije Universiteit Brussel) are acknowledged for experimental support. Part of this work was supported by the Research Priority Area Sustainable Chemistry of the UvA.*

*The authors have declared no conflict of interest.*

## 5 References

- [1] Svec, F., Fréchet, J. M. J., Continuous rods of macroporous polymer as high-performance liquid-chromatography separation media. *Anal. Chem.*, 1992, 64, 820–822.
- [2] Poppe, H., Some reflections on speed and efficiency of modern chromatographic methods. *J. Chromatogr. A*, 1997, 778, 3–21.
- [3] Altmaier, S., Cabrera, K., Structure and performance of silica-based monolithic HPLC columns. *J. Sep. Sci.*, 2008, 31, 2551–2559.
- [4] Svec, F., Fréchet, J. M. J., Temperature, a simple and efficient tool for the control of pore-size distribution in macroporous polymers. *Macromolecules*, 1995, 28, 7580–7582.
- [5] Moravcova, D., Jandera, P., Urban, J., Planeta, J., Characterization of polymer monolithic stationary phases for capillary HPLC. *J. Sep. Sci.*, 2003, 26, 1005–1016.
- [6] Eeltink, S., Herrero-Martinez, J. M., Rozing, G. P., Schoenmakers, P. J., Kok, W. T., Tailoring the morphology of methacrylate ester-based monoliths for optimum efficiency in liquid chromatography. *Anal. Chem.*, 2005, 77, 7342–7347.
- [7] Vaast, A., Terry, H., Svec, F., Eeltink, S., Nanostructured porous polymer monolithic columns for capillary liquid chromatography of peptides. *J. Chromatogr. A*, 2014, 1374, 171–179.
- [8] Gritti, F., Guiochon, G., Mass transport of small retained molecules in polymer-based monolithic columns. *J. Chromatogr. A*, 2014, 1362, 49–61.
- [9] Wouters, B., Vaast, A., Treumann, A., Ursem, M., Ho, J., Hornshaw, M., Raes, M., Terry, H., Eeltink, S., The potential of polymeric monolithic capillary columns for the LC-MS analysis of intact proteins. *LC GC Eur.*, 2012, 25, 10–19.
- [10] Hemstrom, P., Nordborg, A., Irgum, K., Svec, F., Fréchet, J. M. J., Polymer-based monolithic microcolumns for hydrophobic interaction chromatography of proteins. *J. Sep. Sci.*, 2006, 29, 25–32.
- [11] Yamamoto, S., Nakamura, M., Tarmann, C., Jungbauer, A., Retention studies of DNA on anion-exchange monolith chromatography: binding site and elution behavior. *J. Chromatogr. A*, 2007, 1144, 155–160.
- [12] Toll, H., Wintringer, R., Schweiger-Hufnagel, U., Huber, C. G., Comparing monolithic and microparticulate capillary columns for the separation and analysis of peptide mixtures by liquid chromatography-mass spectrometry. *J. Sep. Sci.*, 2005, 28, 1666–1674.
- [13] Petro, M., Svec, F., Gitsov, I., Fréchet, J. M. J., Molded monolithic rod of macroporous poly(styrene-co-divinylbenzene) as a separation medium for HPLC of synthetic polymers: “On-column” precipitation-redissolution chromatography as an alternative to size exclusion chromatography of styrene oligomers and polymers. *Anal. Chem.*, 1996, 68, 315–321. doi:10.1021/ac950726r.
- [14] Maksimova, E., Vlach, E., Sinitsyna, E., Tennikova, T., HPLC analysis of synthetic polymers on short monolithic columns. *J. Sep. Sci.*, 2013, 36, 3741–3749.
- [15] Svec, F., Quest for organic polymer-based monolithic columns affording enhanced efficiency in high performance liquid chromatography separations of small molecules in isocratic mode. *J. Chromatogr. A*, 2012, 1228, 250–262.
- [16] Wang, J. F., Bai, L. G., Wei, Z., Qin, J. X., Ma, Y. M., Liu, H. Y., Incorporation of ionic liquid into porous polymer monoliths to enhance the separation of small molecules in reversed-phase high-performance liquid chromatography. *J. Sep. Sci.*, 2015, 38, 2101–2108.
- [17] Nischang, I., Porous polymer monoliths: morphology, porous properties, polymer nanoscale gel structure and their impact on chromatographic performance. *J. Chromatogr. A*, 2013, 1287, 39–58.
- [18] Urban, J., Current trends in the development of porous polymer monoliths for the separation of small molecules. *J. Sep. Sci.*, 2016, 39, 51–68.
- [19] Shen, Y., Qi, L., Mao, L., Macroporous polymer monoliths with a well-defined three dimensional skeletal morphology derived from a novel phase separator for HPLC. *Polymer*, 2012, 53, 4128–4134.

- [20] Yang, S., Zeng, L., Li, Z., Zhang, X., Liu, H., Nie, C., Liu, H., Tailoring the morphology of emulsion-based (glycidylmethacrylate-divinylbenzene) monoliths. *Eur. Polym. J.*, 2014, 57, 127–136.
- [21] Urban, J., Eeltink, S., Jandera, P., Schoenmakers, P. J., Characterization of polymer-based monolithic capillary columns by inverse size-exclusion chromatography and mercury-intrusion porosimetry. *J. Chromatogr. A*, 2008, 1182, 161–168.
- [22] Hasegawa, G., Kanamori, K., Nakanishi, K., Yamago, S., Fabrication of highly crosslinked methacrylate-based polymer monoliths with well-defined macropores via living radical polymerization. *Polymer*, 2011, 52, 4644–4647.
- [23] Ravikovitch, P. I., Haller, G. L., Neimark, A. V., Density functional theory model for calculating pore size distributions: pore structure of nanoporous catalysts. *Colloid Interface Sci.*, 1998, 76, 203–226.
- [24] Groen, J. C., Peffer, L. A. A., Pérez-Ramírez, J., Pore size determination in modified micro- and mesoporous materials. Pitfalls and limitations in gas adsorption data analysis. *Micropor. Mesopor. Mat.*, 2003, 60, 1–17.
- [25] Thommes, M., Physical adsorption characterization of nanoporous materials. *Chem. Ing. Tech.*, 2010, 82, 1059–1073.
- [26] Thommes, M., Kaneko, K., Neimark, A. V., Oliver, J., Rodríguez-Reinoso, F., Rouquerol, J., Sing, K., Physisorption of gases, with special reference to the evaluation of surface area and pore size distribution. *Pure Appl. Chem.*, 2015, 87, 1051–1069.
- [27] Stassen, C., Desmet, G., Broeckhoven, K., Van Lokeren, L., Eeltink, S., Characterization of polymer monolithic columns for small-molecule separations using total-pore-blocking conditions. *J. Chromatogr. A*, 2014, 1325, 115–120.
- [28] Laher, M., Causon, T. J., Buchberger, W., Hild, S., Nischang, I., Assessing the nanoscale structure and mechanical properties of polymer monoliths used for chromatography. *Anal. Chem.*, 2013, 85, 5645–5649.
- [29] Courtois, J., Szumski, M., Georgsson, F., Irgum, K., Assessing the macroporous structure of monolithic columns by transmission electron microscopy. *Anal. Chem.*, 2007, 79, 335–344.
- [30] Koku, H., Maier R.S. Czymmek, K. J., Schure, M. R., Lenhoff, A. M., Modeling of flow in a polymeric chromatographic monolith. *J. Chromatogr. A*, 2011, 1218, 3466–3475.
- [31] Koku, H., Maier, R. S., Schure, M. R., Lenhoff, A. M., Modeling of dispersion in a polymeric chromatographic monolith. *J. Chromatogr. A*, 2012, 1237, 55–63.
- [32] Jungreuthmayer, C., Steppert, P., Sekot, G., Zankel, A., Reingruber, H., Zanghellini, J., Jungbauer, A., The 3D pore structure and fluid dynamics simulation of macroporous monoliths: high permeability due to alternating channel width. *J. Chromatogr. A*, 2015, 1425, 141–149.
- [33] Müllner, T., Zankel, A., Mayrhofer, C., Reingruber, H., Höltzel, A., Lv, Y., Svec, F., Tallarek, U., Reconstruction and characterization of a polymer-based monolithic stationary phase using serial block-face scanning electron microscopy. *Langmuir*, 2012, 28, 16733–16737.
- [34] Müllner, T., Zankel, A., Lv, Y., Svec, F., Höltzel, A., Tallarek, U., Assessing structural correlations and heterogeneity length scales in functional porous polymers from physical reconstructions. *Adv. Mater.*, 2015, 27, 6009–6013.
- [35] Aggarwal, P., Asthana, V., Lawson, J. S., Tolley, H. D., Wheeler, D. R., Mazzeo, B. A., Lee, M. L., Correlation of chromatographic performance with morphological features of organic polymer monoliths. *J. Chromatogr. A*, 2014, 1334, 20–29.
- [36] Courtois, J., Szumski, M., Byström, E., Iwasiewicz, A., Shchukarev, A., Irgum, K., A study of surface modification and anchoring techniques used in the preparation of monolithic microcolumns in fused silica capillaries. *J. Sep. Sci.*, 2006, 29, 14–24.
- [37] Rouquerol, J., Baron, G. V., Denoyel, R., Giesche, H., Groen, J., Klobes, P., Levitz, P., Neimark, A. V., Rigby, S., Skudas, R., Sing, K., Thommes, M., Unger, K., The characterization of macroporous solids: An overview of the methodology. *Micropor. Mesopor. Mat.*, 2012, 154, 2–6.
- [38] Landers, J., Yu, G. G., Neimark, A. V., Density functional theory methods for characterization of porous materials. *Colloid Surface A*, 2013, 437, 3–32.
- [39] Washburn, E. W., The dynamics of capillary flow. *Phys. Rev.*, 1921, 17, 273–283.
- [40] Wouters, S., Wouters, B., Vaast, A., Terryn, H., Van Assche, G., Eeltink, S., Monitoring the morphology development of polymer-monolithic stationary phases by thermal analysis. *J. Sep. Sci.*, 2013, 37, 179–186.
- [41] Byström, E., Viklund, C., Irgum, K., Differences in porous characteristics of styrenic monoliths prepared by controlled thermal polymerization in molds of varying dimensions. *J. Sep. Sci.*, 2010, 33, 191–199.
- [42] Meyer, K., Klobes, P., Comparison between different presentations of pore size distribution in porous materials. *J. Fresenius Anal. Chem.*, 1999, 363, 174–178.
- [43] Sing, K., Everett, D. H., Haul, R. A. W., Moscou, L., Pierotti, R. A., Rouquerol, J., Siemieniewska, T., Reporting physisorption data for gas/solid systems with special reference to the determination of surface area and porosity. *Pure Appl. Chem.*, 1985, 57, 603–619.
- [44] Guan, Y., Zhou, L., Shang, Z., Dry-packed capillary columns for micro HPLC. *J. High Res. Chromatogr.*, 1992, 15, 434–436.
- [45] Billen, J., Desmet, G., Understanding and design of existing and future chromatographic support formats. *J. Chromatogr. A*, 2007, 1168, 73–99.
- [46] Cabral, J. L., Bandilla, D., Skinner, C. D., Pore size characterization of monolith for electrochromatography via atomic force microscopy studies in air and liquid phase. *J. Chromatogr. A*, 2006, 1108, 83–89.
- [47] Nischang, I., Brüggemann, O., On the separation of small molecules by means of nano-liquid chromatography with methacrylate-based macroporous polymer monoliths. *J. Chromatogr. A*, 2010, 1217, 5389–5397.
- [48] Eeltink, S., Gzil, P., Kok, W. T., Schoenmakers, P. J., Desmet, G., Selection of comparison criteria and experimental conditions to evaluate the kinetic performance of monolithic and packed-bed columns. *J. Chromatogr. A*, 2006, 1130, 108–114.